Identifying the biological control of the annual and multi-year variations in South Atlantic air-sea CO_2 flux

Daniel J. Ford[1,2], Gavin H. Tilstone[1], Jamie D. Shutler[2] and Vassilis Kitidis[1]

[1] Plymouth Marine Laboratory, Plymouth, UK
[2] College of Life and Environmental Sciences, University of Exeter, Penryn, UK

Correspondence to: Daniel Ford (dfo@pml.ac.uk)

Abstract. The accumulation of anthropogenic CO_2 emissions in the atmosphere has been buffered by the absorption of CO_2 by the global ocean which acts as a net CO_2 sink. The CO_2 flux between the atmosphere and the ocean, that collectively results in the oceanic carbon sink, is spatially and temporally variable, and fully understanding the driving mechanisms behind this flux is key to assessing how the sink may change in the future. In this study a time series decomposition analysis was applied to satellite observations to determine the drivers that control the sea-air difference of CO_2 partial pressure ($\Delta p CO_2$) and the CO_2 flux on seasonal and interannual time scales in the South Atlantic Ocean. Linear trends in $\Delta p CO_2$ and the CO_2 flux were calculated to identify key areas of change.

Seasonally, changes in both the $\Delta p CO_2$ and CO_2 flux were dominated by sea surface temperature (SST) in the subtropics (north of 40 °S) and were correlated with biological processes in the subpolar regions (south of 40 °S). In the Equatorial Atlantic, analysis of the data indicated that biological processes are likely a key driver, as a response to upwelling and riverine inputs. These results highlighted that seasonally $\Delta p CO_2$ can act as an indicator to identify drivers of the CO_2 flux. Interannually, the SST and biological contributions to the CO_2 flux in the subtropics were correlated with the Multivariate ENSO Index (MEI) which leads to a weaker (stronger) CO_2 sink in El Niño (La Niña) years.

The 16-year time-series identified significant trends in $\Delta p CO_2$ and CO_2 flux, however, these trends were not always consistent in spatial extent. Therefore, predicting the oceanic response to climate change requires the examination of CO_2 flux rather than $\Delta p CO_2$. Positive CO_2 flux trends (weakening sink for atmospheric CO_2) were identified within the Benguela upwelling system, consistent with increased upwelling and wind speeds. Negative trends in the CO_2 flux (intensifying sink for atmospheric CO_2) offshore into the South Atlantic Gyre, were consistent with an increase in the export of nutrients ~~in~~ from mesoscale features, which drives the biological drawdown of CO_2. These multi-year trends in the CO_2 flux indicate that the biological contribution to changes in the air-sea CO_2 flux cannot be overlooked when scaling up to estimates of the global ocean carbon sink.

1 Introduction

Since the industrial revolution, anthropogenic CO_2 emissions have increased unabated and continue to rise atmospheric CO_2
concentrations (IPCC, 2021). The global oceans have buffered the rise by acting as a sink for atmospheric CO_2 at a rate of
between 1 and 3.5 Pg C yr^{-1} (e.g. Friedlingstein et al., 2020; Landschützer et al., 2014; Watson et al., 2020). The strength of
the ocean as a sink for CO_2 appears to be increasing with time (Friedlingstein et al., 2020; Watson et al., 2020). Regionally
this can vary hugely, however, and the ocean can oscillate between a source or sink of atmospheric CO_2. The difference in
the partial pressure of CO_2 (pCO_2) between the seawater and atmosphere (ΔpCO_2) is used as an indicator or proxy, for the
net direction of air-sea CO_2 flux during gas exchange.

In the open ocean, changes in physical and biogeochemical processes that control seawater pCO_2 ($pCO_{2\ (sw)}$) also modify
ΔpCO_2 as the atmospheric pCO_2 ($pCO_{2\ (atm)}$) is less variable (e.g. Henson et al., 2018; Landschützer et al., 2016). ΔpCO_2 can
therefore be controlled by changes in sea surface temperature (SST), because the pCO_2 is proportional to the temperature. In
addition, plankton net community production (NCP) modifies the concentration of CO_2 in the seawater depending on the
balance between net primary production (NPP; uptake of CO_2 via photosynthesis) and respiration (release of CO_2 into the
water). The NCP describes the overall metabolic balance of the plankton community, where positive (negative) NCP
indicates a drawdown (or release) of CO_2 from (or into) the water contributing to a decrease (increase) in ΔpCO_2. Physical
processes, including riverine input (e.g. Ibánhez et al., 2016; Lefèvre et al., 2020; Valerio et al., 2021), and upwelling (e.g.
González-Dávila et al., 2009; Lefèvre et al., 2008; Santana-Casiano et al., 2009) can alter $pCO_{2\ (sw)}$ and ΔpCO_2 directly
through the entrainment of high-CO_2 water or indirectly by modifying NCP through nutrient supply (enhancing
photosynthesis) and/or organic material supply (enhancing respiration).

The air-sea CO_2 flux is more precisely a function of the difference in CO_2 concentrations across the mass boundary layer at
the ocean's surface, with any turbulent exchange characterised by the gas transfer velocity. The CO_2 concentration difference
is determined by the pCO_2 at the base ($pCO_{2\ (sw)}$) and top ($pCO_{2\ (atm)}$) of the mass boundary layer and the respective
solubilities (Weiss, 1974), and must be carefully calculated due to vertical thermo-haline gradients existing across the mass
boundary layer (Woolf et al., 2016). The gas transfer velocity is usually parameterised as a function of wind speed (e.g. Ho
et al., 2006; Nightingale et al., 2000; Wanninkhof, 2014) which accounts for ~75% of the variance in surface turbulent
exchange (e,g, Dong et al., 2021; Ho et al., 2006). Therefore, both oceanographic and meteorological conditions are able to
modify and control the seasonality, interannual variability and multi-year trends of this flux.

Seasonal drivers of ΔpCO_2 have been explored globally (Takahashi et al., 2002), and regionally in the Atlantic Ocean
(Landschützer et al., 2013; Henson et al., 2018). Takahashi et al. (2002) used binned *in situ* $pCO_{2\ (sw)}$ observations to a 4° by
5° global grid, and found that SST drives ΔpCO_2 in the subtropics, and non-SST processes (i.e. biological activity and ocean
circulation) dominate in subpolar and equatorial regions. Landschützer et al. (2013) used a self-organising map feed forward
neural network (SOM-FNN) technique to extrapolate the *in situ* $pCO_{2\ (sw)}$ observations and reported similar seasonal drivers
in the Atlantic Ocean with one exception, that SST and non-SST processes compensated each other in the Equatorial

Atlantic. Henson et al. (2018) using binned *in situ* observations for the North Atlantic Ocean, also indicated that the subtropics are driven by SST and that subpolar regions are correlated with biological activity.

The interannual drivers of ΔpCO_2 are different compared to the seasonal drivers in the North Atlantic (Henson et al., 2018), which could be true of the South Atlantic Ocean, though this needs to be further investigated. Landschützer et al. (2016, 2014) postulated the El Niño cycle may influence ΔpCO_2 in the subtropical South Atlantic but did not explore the underlying processes. South of 35° S, Landschützer et al. (2015) indicated that atmospheric forcing could control the interannual variability of ΔpCO_2 through changes in Ekman transport and upwelling. These interannual drivers of ΔpCO_2 and the CO_2 flux in the South Atlantic Ocean are poorly understood but have key implications for determining how the oceanic CO_2 sink could be impacted by climate change and its evolution over interannual and decadal timescales.

In this study, we investigate the drivers of ΔpCO_2 and the CO_2 flux in the South Atlantic Ocean over both seasonal and interannual timescales using a timeseries decomposition approach. Trends in ΔpCO_2 and the CO_2 flux were calculated from 2002 to 2018, and regions in the South Atlantic Ocean showing the greatest change in the CO_2 flux are investigated.

2. Data and Methods

2.1. pCO_2 data

Satellite estimates of pCO_2 (sw) were retrieved from the South Atlantic Feed Forward Neural Network (SA-FNN) dataset (Ford et al., 2022, 2021a). Ford et al. (2022) showed that the SA-FNN improved on estimating the seasonal pCO_2 (sw) variability in the South Atlantic Ocean compared to the current estimates using the 'state of the art' methodology (the SOM-FNN). The SA-FNN estimates pCO_2 (sw) by clustering *in situ* monthly 1° gridded Surface Ocean CO_2 Atlas (SOCAT) v2020 pCO_2 (sw) observations (Bakker et al., 2016; Sabine et al., 2013), that have been reanalysed into a dataset configured using consistent depth and temperature fields (Goddijn-Murphy et al., 2015; Woolf et al., 2016; Reynolds et al., 2002), into eight static provinces in the South Atlantic Ocean (Fig. B1a). The use of eight static provinces allows the SA-FNN to more accurately reproduce the pCO_2 (sw) variability. The nonlinear relationships between pCO_2 (sw) and three environmental drivers; (SST, NCP and pCO_2 (atm)), were constructed for each province with a feed forward neural network (FNN). The FNN for each province were applied to produce spatially and temporally complete pCO_2 (sw) fields on monthly 1° grids between July 2002 and December 2018, with uncertainties also generated on a per pixel basis as described in Ford et al. (2022). These per pixel uncertainties are displayed shown in Appendix B (Fig. B1).

Monthly 1° grids of pCO_2 (atm) were extracted from v5.5 of the global estimates of pCO_2 (sw) dataset (Landschützer et al., 2017, 2016) which was calculated using the dry mixing ratio of CO_2 from the NOAA-ESRL marine boundary layer reference (https://www.esrl.noaa.gov/gmd/ccgg/mbl/; last accessed 25/09/2020), Optimum Interpolated SST (Reynolds et al., 2002) and sea level pressure following Dickson et al. (2007). ΔpCO_2 was calculated from pCO_2 (sw) and pCO_2 (atm) as;

$$\Delta pCO_2 = pCO_2\,_{(sw)} - pCO_2\,_{(atm)} \tag{1}$$

2.2. Air-sea CO₂ flux data

The air-sea CO_2 flux (F) can be estimated using a bulk parameterisation as:

$$F = k \left(\alpha_W \, pCO_{2\,(sw)} - \alpha_s \, pCO_{2\,(atm)} \right) \tag{2}$$

Where k is the gas transfer velocity which was estimated from ERA5 monthly reanalysis wind speed (Hersbach et al., 2019) following the parameterisation of Nightingale et al. (2000). α_w and α_s are the solubility of CO_2 at the base and top of the mass boundary layer at the sea surface (Woolf et al., 2016). α_w was calculated as a function of SST and sea surface salinity (SSS) (Weiss, 1974) using the monthly Optimum Interpolated SST (Reynolds et al., 2002) and SSS from the Copernicus Marine Environment Modelling Service global ocean physics reanalysis product (GLORYS12V1; CMEMS, 2021). α_s was calculated using the same temperature and salinity datasets but included a gradient from the base to the top of mass boundary layer of -0.17 K (Donlon et al., 1999) and +0.1 salinity units (Woolf et al., 2016). $pCO_{2\,(atm)}$ was calculated using the dry mixing ratio of CO_2 from the NOAA-ESRL marine boundary layer reference, Optimum Interpolated SST (Reynolds et al., 2002) applying a cool skin bias (0.17K; Donlon et al., 1999) and sea level pressure following Dickson et al. (2007).

All of these calculations along with the resulting monthly CO_2 flux were carried out using the open source FluxEngine toolbox (Holding et al., 2019; Shutler et al., 2016), for the period between July 2002 and December 2018, assuming 'rapid' transfer (as described in Woolf et al., 2016).

2.3. Biological data

The 4 km resolution mean monthly chlorophyll-*a* (Chl *a*) was calculated from Moderate Resolution Imaging Spectroradiometer on Aqua (MODIS-A) Level 1 granules, retrieved from the National Aeronautics Space Administration (NASA) Ocean Colour website (https://oceancolor.gsfc.nasa.gov/; last accessed 10/12/2020), using SeaDAS v7.5, and applying the standard OC3-CI algorithm for Chl *a* (https://oceancolor.gsfc.nasa.gov/atbd/chlor_a/; last accessed 15/12/2020). Monthly composites of MODIS-A SST (NASA OBPG, 2015) and photosynthetically active radiation (PAR; NASA OBPG, 2017b) were also downloaded from the NASA Ocean Colour website. Monthly NPP composites were generated from MODIS-A Chl *a*, SST and PAR composites using the Wavelength Resolving Model (Morel, 1991) with the look up table described in Smyth et al. (2005). Coincident monthly composites of NCP using the algorithm NCP-D described in Tilstone et al. (2015) were generated using the NPP and SST data. Further details of the satellite algorithms are given in O'Reilly et al. (1998), O'Reilly and Werdell (2019) and Hu et al. (2012) for Chl *a*, Smyth et al. (2005), Tilstone et al. (2005, 2009) for NPP and Tilstone et al. (2015) for NCP. Monthly composites were generated between July 2002 and December 2018 and were re-gridded onto the same 1° grid as the $pCO_{2\,(sw)}$ and flux data. Ford et al. (2021b) showed that these satellite algorithms for Chl *a*, NPP, NCP and SST are accurate compared to *in situ* observations in the South Atlantic Ocean following an algorithm intercomparison which accounted for model, *in situ* and input parameter uncertainties.

2.4. Seasonal and interannual driver analysis

The X-11 analytical econometric tool (Shiskin et al., 1967) was used to decompose the timeseries into seasonal, interannual and residual components following the methodology of Pezzulli et al. (2005). In brief, the X-11 method comprises a three step filtering algorithm:; (1) The interannual component (T_t) is initially estimated using an annual centred running mean, which is subtracted from the initial timeseries (X_t) to estimate the seasonal component (S_t). (2) T_t is revised by applying an annual centred running mean to the X_t minus S_t. The revised T_t is removed from X_t and the final S_t calculated. (3) The final T_t is calculated by applying an annual centred running mean to X_t minus the revised S_t. The analysis has been shown to be effective in the decomposition of environmental time-series (Pezzulli et al., 2005; Vantrepotte & Mélin, 2011; Henson et al., 2018), that allows the seasonal cycle to vary on a yearly basis and, produces an interannual component that results in a robust representation of the longer-term changes in the timeseries.

The approach was applied to monthly 1° fields of ΔpCO_2 that were estimated from $pCO_{2\,(atm)}$ and SA-FNN $pCO_{2\,(sw)}$, on a per pixel basis. The $pCO_{2\,(atm)}$ and spatially and temporally varying $pCO_{2\,(sw)}$ uncertainties (Table 1; Fig. B1) were propagated through the X-11 analysis, using a Monte Carlo uncertainty propagation approach. The input time series were randomly perturbed 1000 times within the uncertainties of each parameter, and Spearman correlations calculated for each perturbation. The 95% confidence interval was extracted from the resulting distribution of correlations coefficients, and results were deemed significant ($\alpha < 0.05$) where the confidence interval remained significant. Spatial autocorrelation was tested using the method of field significance (Wilks, 2006). The analysis was then conducted on the CO_2 fluxes, on a per pixel basis. The $pCO_{2\,(sw)}$, $pCO_{2\,(atm)}$, gas transfer velocity, SST and SSS uncertainties (Table 1) were propagated through the flux calculations using the same Monte Carlo uncertainty propagation approach used for ΔpCO_2.

The potential drivers tested were MODIS-A skin SST, NCP and NPP alongside SSS from the CMEMS global reanalysis product (GLORYSV12; CMEMS, 2021) and two climate indices: Multivariate ENSO Index (MEI) as an indicator of El Niño Southern Oscillation phases, https://www.esrl.noaa.gov/psd/enso/mei (last accessed: 19/12/2019); Southern Annular Mode (SAM) data, which indicate the displacement of the westerly winds in the Southern Ocean, were downloaded from http://www.nerc-bas.ac.uk/icd/gjma/sam.html (last accessed: 19/12/2019).

Table 1: Uncertainties in the input parameters used in the Monte Carlo uncertainty propagation.

Parameter	Uncertainty	Reference
$pCO_{2\,(sw)}$	Variable (Appendix B)	(Ford et al., 2022)
SST	0.441 °C	(Ford et al., 2021b)
SSS	0.1 psu	(Jean-Michel et al., 2021)
$pCO_{2\,(atm)}$	1 µatm	(Takahashi et al., 2009)
Gas transfer velocity	20 %	(Woolf et al., 2019)

2.5. Trend analysis

150 The linear trend in the interannual components of $\Delta p CO_2$ and the CO_2 flux were calculated on a per pixel basis using the non parametric Mann-Kendall test ~~for trend~~ (Kendall, 1975; Mann, 1945) and Sen's Slope estimates (Sen, 1968), which are less sensitive to outliers in the timeseries. The input parameter uncertainties (Table 1) were propagated within this trend analysis using a Monte Carlo uncertainty propagation ($n = 1000$) to extract the 95% confidence interval on the trends. The overall trend was deemed significant if 95% of the trends were significant ($\alpha = 0.05$), and the uncertainties in these trends are
155 displayed in Appendix B (Fig. B2).

2.6. Limitations

It should be noted that correlations between the $\Delta p CO_2$ and SST/NCP are expected since the SA-FNN estimates $p CO_{2\,(sw)}$ (the major determinant of $\Delta p CO_2$ variability) using SST and NCP as input parameters which are subsequently interpreted as drivers here. By extension, but to a lesser extent, this also applies to correlations between CO_2 flux and SST/NCP since $p CO_2$
160 $_{(sw)}$ is included in the flux calculations. Different lines of evidence suggest that this is not a major limitation of our study. Firstly, any correlation between $\Delta p CO_2$/CO_2 flux and SST/NCP is not determined *a priori*, but is an emerging property of the SA-FNN. Therefore, the driver analysis undertaken here represents an indirect decomposition of the SA-FNN drivers rather than a strict correlation analysis between independent variables. The accurate representation of seasonal $p CO_{2\,(sw)}$ cycles across the South Atlantic Ocean (Ford et al., 2022) provides confidence in the SA-FNN. Secondly, conducting the analysis
165 described by Henson et al. (2018) using *in situ* $p CO_{2\,(sw)}$ to estimate $\Delta p CO_2$ on a per province basis (Longhurst, 1998) for the South Atlantic Ocean, yielded similar seasonal drivers to the SA-FNN (Appendix A). The interannual drivers displayed some differences however, which may be due to the spatial and temporal averaging that is required to construct the in situ timeseries.

3. Results

170 **3.1. Seasonal drivers of $\Delta p CO_2$ and CO_2 flux**

The X-11 analysis conducted on $\Delta p CO_2$ indicated significant seasonal correlations (Fig. 1), when the uncertainties are accounted for. The subtropics (10-°_S to 40-°_S) showed positive correlations between $\Delta p CO_2$, SST and SSS (Fig. 1c, d), as well as negative correlations between $\Delta p CO_2$, NCP and NPP (Fig. 1a, b). In contrast the subpolar (south of 40-°_S) and equatorial regions (10-°_N to 10-°_S) displayed negative correlations between $\Delta p CO_2$ and SST (Fig. 1c). Correlations
175 between $\Delta p CO_2$ and NCP were negative in the subpolar regions and were positive in the Equatorial regions (Fig. 1a). There were no significant correlations observed between $\Delta p CO_2$ and MEI or SAM in any of the regions.
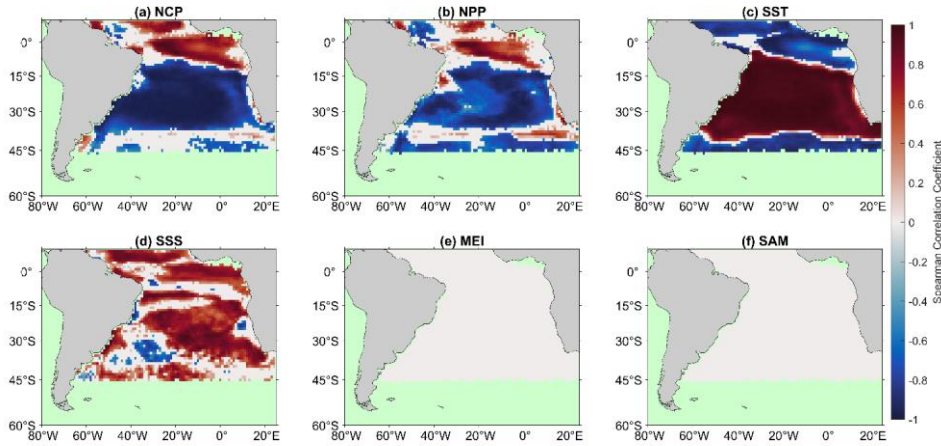
Figure 1: Significant Spearman correlations between the ΔpCO$_2$ seasonal component of the X-11 analysis and (a) net community production (NCP), (b) net primary production (NPP), (c) sea surface temperature (SST), (d) sea surface salinity (SSS), (e) Multivariate ENSO index (MEI) and (f) Southern Annular Mode (SAM) seasonal components. White regions indicate no significant correlations, and green regions indicate no analysis was performed due to missing satellite data.

Regional deviations were observed in the Amazon Plume, Benguela upwelling, the South American coast, and a band across 40–°_S. The region under the influence of the Amazon Plume indicated negative correlations between ΔpCO$_2$ and NCP in contrast to the surrounding waters which had positive correlations (Fig. 1a). The Benguela upwelling displayed positive correlations between ΔpCO$_2$ and NCP (Fig. 1a), no significant correlations between ΔpCO$_2$ and SST (Fig. 1c), and negative correlations between ΔpCO$_2$ and SSS (Fig. 1e). The South American coast between 12–°_S and 17–°_S displayed positive correlations between ΔpCO$_2$ and NPP (Fig. 1b), along with negative correlations between ΔpCO$_2$ and SSS (Fig. 1e). Negative correlation between ΔpCO$_2$ and SSS, and positive correlations between NCP, NPP and ΔpCO$_2$ were also observed in the southwestern Atlantic (Fig. 1e). Positive correlations between NCP, NPP and ΔpCO$_2$ were identified in a band across 40–°_S (Fig. 1a, b). Performing the X-11 analysis on the CO$_2$ flux revealed similar and comparable correlations to ΔpCO$_2$ (Fig. 2). Significant driver-flux correlations were observed over a larger area however, compared to ΔpCO$_2$.
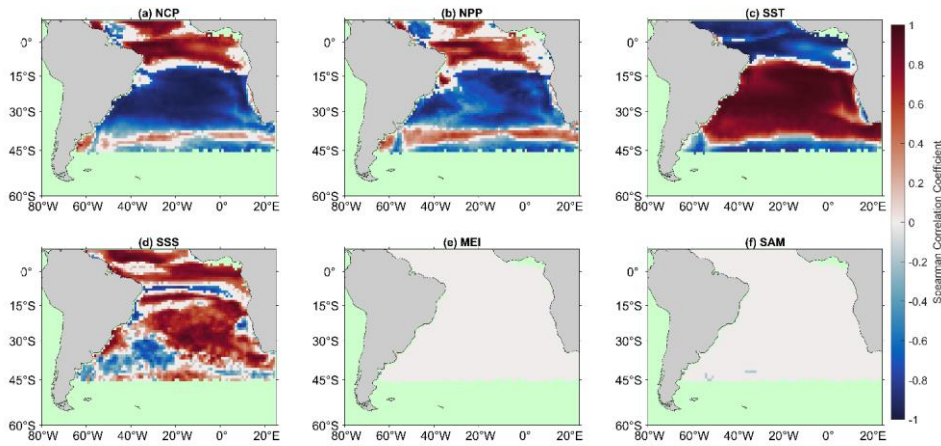
Figure 2: Significant Spearman correlations between the air-sea CO$_2$ flux seasonal component of the X-11 analysis and (a) net community production (NCP), (b) net primary production (NPP), (c) sea surface temperature (SST), (d) sea surface salinity (SSS), (e) Multivariate ENSO index (MEI) and (f) Southern Annular Mode (SAM) seasonal components. White regions indicate no significant correlations, and green regions indicate no analysis was performed due to missing satellite data.

3.2. Interannual drivers of ΔpCO$_2$ and CO$_2$ flux

The X-11 analysis identified regionally significant interannual correlations between ΔpCO$_2$ and SST, MEI and to a lesser extent NCP and SSS (Fig. 3). The subtropics displayed positive correlations between SST and ΔpCO$_2$, which extended across the basin from the South American coast (Fig. 3c). Positive correlations were also observed between the MEI and ΔpCO$_2$ (Fig. 3e), with a similar geographic extent as the correlations with SST. In the central South Atlantic gyre spatially variable negative correlations between NCP and ΔpCO$_2$, and positive correlations between SSS and ΔpCO$_2$ were observed (Fig. 3a, d). The central Equatorial Atlantic displayed spatially variable positive correlations between NCP and ΔpCO$_2$, which extended south-east towards the African coast (Fig. 3a).
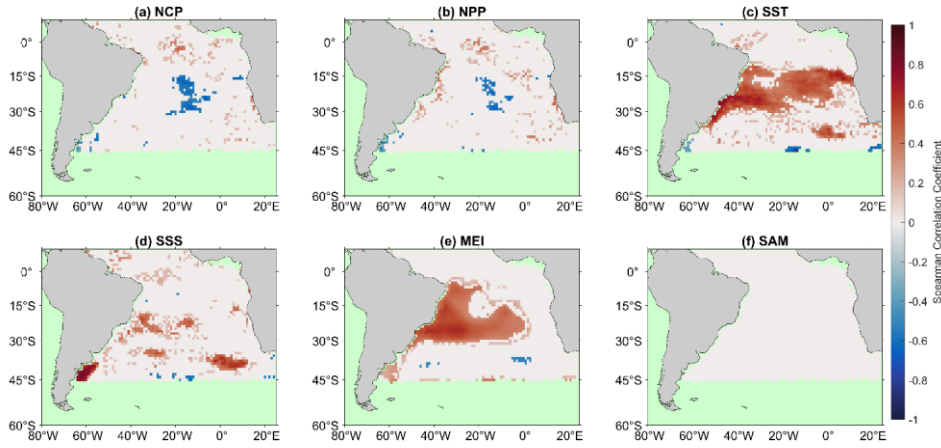
Figure 3: Significant Spearman correlations between the ΔpCO₂ interannual component of the X-11 analysis and (a) net community production (NCP), (b) net primary production (NPP), (c) sea surface temperature (SST), (d) sea surface salinity (SSS), (e) Multivariate ENSO index (MEI) and (f) Southern Annular Mode (SAM) interannual components. White regions indicate no significant correlations, and green regions indicate no analysis was performed due to missing satellite data.

Significant interannual correlations for the CO_2 flux were also identified by the X-11 analysis (Fig. 4), which generally covered a larger spatial area to the corresponding ΔpCO_2 correlations (Fig. 3). Positive correlations between the CO_2 flux and SST were observed in the subtropics (Fig. 4c), consistent with the correlations with ΔpCO_2 (i.e. by comparing Fig. 4c and Fig. 3c). Nevertheless, negative correlations between the CO_2 flux and SST were observed at the border between the equatorial region and subtropics, which was not identified in the ΔpCO_2 correlations. Negative correlations between NCP and the CO_2 flux were also identified over a spatially larger area (Fig. 4a, 3a). Correlations between the MEI and CO_2 flux were positive in the subtropics (Fig. 4e) and included a band of negative correlations to the south between 35-° S and 45-° S (Fig. 4e).

Positive correlations between NCP and CO_2 flux were observed in the western equatorial Atlantic, alongside spatially variable negative correlations to SST (Fig. 4a, c). Positive correlations between SSS and CO_2 flux were identified in the region of the Amazon plume (Fig. 4d). Weak positive correlations between the SAM and CO_2 flux were identified between 30° S and 45° S (Fig. 4f).
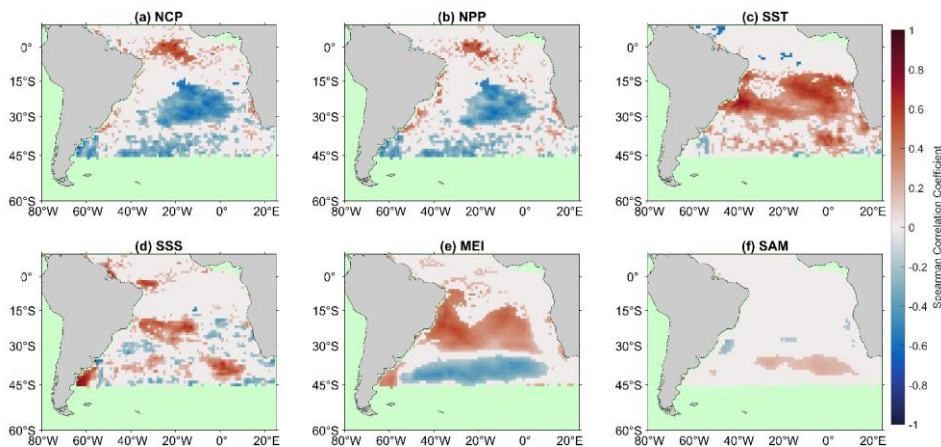
Figure 4: Significant Spearman correlations between the air-sea CO₂ flux interannual component of the X-11 analysis and (a) net community production (NCP), (b) net primary production (NPP), (c) sea surface temperature (SST), (d) sea surface salinity (SSS), (e) Multivariate ENSO index (MEI) and (f) Southern Annular Mode (SAM) interannual components. White regions indicate no significant correlations, and green regions indicate no analysis was performed due to missing satellite data.

3.3. Trends in interannual ΔpCO₂ and CO₂ flux

Regions of significant trends in the interannual component of $\Delta p\text{CO}_2$ were observed (Fig. 5a). Negative trends occurred in the South Atlantic gyre. Positive trends in $\Delta p\text{CO}_2$ were identified along the South African coast, which switched to strong negative trends moving offshore into the central South Atlantic gyre. Positive trends were also observed in the Equatorial Atlantic consistent with the positions of the Amazon Plume and Equatorial Upwelling.

Regions of significant trends in the CO₂ flux were identified (Fig. 5b), but over much larger spatial areas than evident in the $\Delta p\text{CO}_2$ results (i.e. comparing Fig. 5a with 5b). The trends in CO₂ flux are generally in the same direction as trends in $\Delta p\text{CO}_2$. Strong positive trends in the CO₂ flux occurred in the Benguela upwelling region, before switching to a negative trend offshore of similar magnitude but occupying a larger spatial extent.

240
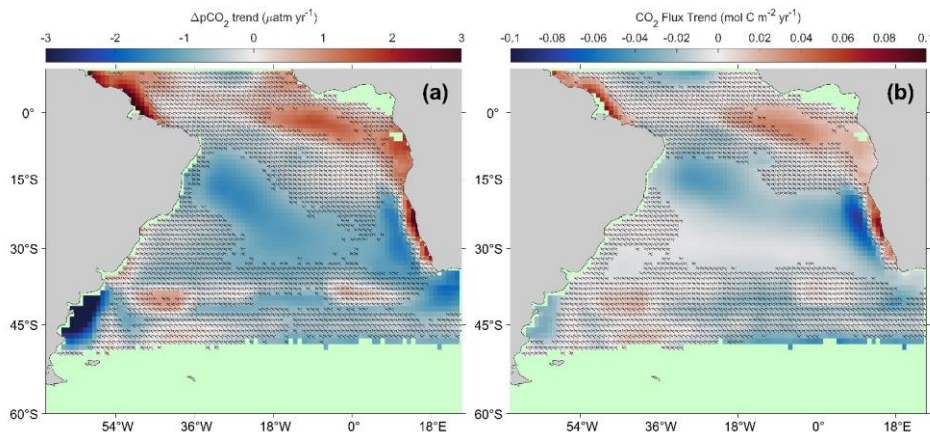
Figure 5: Linear trends in (a) $\Delta p CO_2$ and (b) the air-sea CO_2 flux between 2002 and 2018. Hashed areas indicate non-significant trends when accounting for the uncertainties. Green regions indicate insufficient data to calculate trends.

4. Discussion

4.1. Seasonal drivers of $\Delta p CO_2$ and CO_2 flux

245   Previous studies have explored the seasonal drivers of $\Delta p CO_2$ and to a lesser extent the air-sea CO_2 flux–. In this study, we investigated the drivers of $\Delta p CO_2$ and CO_2 flux at both seasonal and interannual timescales in the South Atlantic Ocean. In the North Atlantic, Henson et al. (2018) indicated that the seasonal variability in subtropical $\Delta p CO_2$ variability is driven by SST, whereas the variability in $\Delta p CO_2$ in subpolar regions is biologically driven, similar to previous studies (Takahashi et al., 2002; Landschützer et al., 2013). The X-11 analysis conducted on spatially complete $\Delta p CO_2$ and CO_2 flux displayed

250   consistent seasonal results (Fig. 1, 2), though for the CO_2 flux significant correlations occupied a larger area. These both indicated a similar pattern in seasonal drivers for the South Atlantic Ocean, with subtropical $\Delta p CO_2$ and CO_2 flux driven by SST, and subpolar correlated with biological controls, although the equatorial region exhibited more complex patterns (Fig. 1).

    In the Equatorial Atlantic, the correlations between $\Delta p CO_2$, SST and biological production were spatially variable (Fig. 1).

255   Landschützer et al. (2013) suggested that the temperature and non-temperature (i.e. biological and circulation) drivers generally compensated each other. We found positive correlations between the NCP, $\Delta p CO_2$ and CO_2 flux seasonal components, indicating that biological activity is likely a key driver of seasonal variability in response to the equatorial

upwelling. Ford et al. (2022) showed that the SA-FNN improved the seasonal $pCO_{2\ (sw)}$ variability in the Equatorial Atlantic compared to the current 'state of the art' SOM-FNN methodology (Watson et al., 2020). Elevated ΔpCO_2 associated with elevated NCP in the eastern Equatorial Atlantic was consistent with the seasonal equatorial upwelling (Radenac et al., 2020). Parard et al. (2010) indicated strong negative correlations between SST and ΔpCO_2 during the upwelling season (R= -0.76 for June to September), which is also consistent with our results. By contrast, Lefèvre et al. (2016) showed that correlations between $pCO_{2\ (sw)}$ and SST were weak across the whole year (R= -0.13), and SSS (R = 0.93) was the primary driver at the same station.

In the western Equatorial Atlantic, negative correlations between NCP and ΔpCO_2, and positive correlations between the SSS and ΔpCO_2 seasonal component occurred in the vicinity of the Amazon River mouth. The mixing of the Amazon river and oceanic water decreases SSS (Ibánhez et al., 2016; Lefèvre et al., 2020; Bonou et al., 2016; Lefévre et al., 2010), and increases the nutrient supply to the ocean which can in turn enhance NPP and NCP, leading to a decrease in ΔpCO_2 within the Amazon plume (Körtzinger, 2003; Cooley et al., 2007). This coupling produces an extensive area of depressed ΔpCO_2 which is a CO_2 sink (Ibánhez et al., 2016). Lefèvre et al. (2010) indicated that rainfall from the intertropical convergence zone could reduce SSS, with an associated decrease in ΔpCO_2. The Eastern Tropical Atlantic is also subject to large river input, especially from the Congo (Hopkins et al., 2013) and Niger rivers, which could produce nutrient-rich plumes that fuel NCP and decrease ΔpCO_2 (Lefèvre et al., 2016, 2021).

Between 30–° S and 45–° S, dissolved inorganic carbon and SST exert a similar influence on $pCO_{2\ (sw)}$, indicating that seasonal changes in dissolved inorganic carbon driven by biological uptake in the summer and upwelling in winter are approximately balanced by seasonal changes in SST and their control on the solubility pump (Henley et al., 2020). This likely explains the band of positive correlations between NCP, NPP and ΔpCO_2 and sharp transitions in correlations between SST and ΔpCO_2 across ~40–° S.

Deviations from the expected drivers in the subtropics, occurred within the Benguela upwelling system between 20–° S and 35–° S. Positive correlations between NCP and the CO_2 flux (Fig. 2a) alongside negative correlations between SST, SSS and the CO_2 flux (Fig. 2c, d) are indicative of upwelled waters that have both elevated $pCO_{2\ (sw)}$ and nutrients, which cause an increase in NPP (Lamont et al., 2014). These upwelled waters move offshore in filaments (Rubio et al., 2009) where NPP decreases, and SST becomes the dominant driver, which is confirmed by the positive correlations between SST and the CO_2 flux further offshore. Ford et al. (2021b) indicated a switch in NCP drivers in the Benguela upwelling from wind driven upwelling on the shelf, to filaments that propagate offshore from the upwelling front, which is consistent with the switch in the drivers observed for the CO_2 flux as these filaments move offshore.

At between 12° S and 17 °S along the South American coast, there were also deviations from the expected drivers as there were positive correlations between NPP and ΔpCO_2 (Fig. 1b) and negative correlations between SSS and ΔpCO_2 (Fig. 1d), which are consistent with an upwelling signature that occurs along the coast. Aguiar et al. (2018) also showed intense seasonal upwelling events in this region that are driven by wind and currents. The southern coast of South America is strongly influenced by riverine water input that reduces the total alkalinity and therefore causes an increase in $pCO_{2\ (sw)}$

(Liutti et al., 2021). This is associated with an increased supply of nutrients which in turn enhances NPP, though the main drivers of $pCO_{2\ (sw)}$ in this region still remain as total alkalinity and SST (Liutti et al., 2021). This potentially explains the positive correlation between ΔpCO_2 and both NCP and NPP (Fig. 1a, b), as well as the negative correlations between ΔpCO_2

295 and SSS. The extension offshore of this negative correlation between SSS and ΔpCO_2 (Fig. 1d) could be caused by the advection of water masses due to intense mesoscale eddy activity arising from the Brazil-Malvinas confluence (Mason et al., 2017).

The seasonal correlations between the CO_2 flux and the drivers were similar to ΔpCO_2, but for CO_2 flux these occurred over a larger spatial area. The South Atlantic subtropical anticyclone (Reboita et al., 2019) which controls wind speeds across the

300 region, and therefore the gas transfer velocity, could enhance the CO_2 flux into the subtropical ocean, through higher (or lower) wind speeds in winter (or summer; Xiong et al., 2015). Since seasonal variations in ΔpCO_2 largely explain the seasonal variability in the CO_2 flux, ΔpCO_2 can be used as a proxy to understand seasonal variations in the CO_2 flux in this region.

4.2. Interannual drivers of ΔpCO_2 and CO_2 flux

305 The larger geographic region of significant correlations for the air-sea CO_2 flux compared to ΔpCO_2, and the consistency between the two results (i.e. comparing the smaller regions of ΔpCO_2 correlations with their equivalent in the flux results; Fig. 3, 4) suggests that analysing the CO_2 flux is the better dataset to investigate drivers of variations in inter-annual and longer timescales. The results become clearer when analysing the CO_2 flux, where the effects of solubility and gas transfer (estimated via wind speed proxy) could reinforce correlations and multi-year trends, which will be retrieved by performing

310 long timeseries analyses on the CO_2 flux. Landschützer et al. (2015) showed that variations in the Southern Ocean carbon sink were primarily driven by changes in ΔpCO_2, when integrating across basin scales. At localised scales of 1° by 1° as performed in our analysis, changes in surface turbulence and solubility are shown to be important in determining interannual variability, consistent with Keppler and Landschützer (2019). In the North Atlantic Ocean, Henson et al. (2018) showed that the seasonal and interannual drivers of ΔpCO_2 are different, which could arise from the necessity to study CO_2 fluxes over

315 longer timescales.

The interannual component of NCP and the CO_2 flux were negatively correlated in the subtropical gyre (Fig. 4a), alongside a positive correlation between SST and CO_2 flux (Fig. 4b). El Niño (La Niña) events are known to influence the South Atlantic Ocean, causing an increase (decrease) in SST across the basin (Rodrigues et al., 2015; Colberg et al., 2004), and a decrease (increase) in NPP and NCP (Ford et al., 2021b; Tilstone et al., 2015). Positive correlations between the MEI and CO_2 flux

320 (Fig. 4e) indicate that the MEI partially controls the interannual variability in CO_2 flux in the South Atlantic subtropical gyre, through modulations primarily in SST and to a lesser extent NCP. The South Atlantic Subtropical Anticyclone has been observed to strengthen (weaken) and move south (north) during La Niña (El Niño) events. This displacement increases (decreases) wind speeds across the subtropical South Atlantic, which will enhance (weaken) gas exchange, and elevate

(depress) NCP (Ford et al., 2021b). These results suggest a more significant role of NCP in controlling the interannual
variability in the CO_2 flux than has previously been thought.

The negative correlation between the CO_2 flux and the MEI in a band between 30° S and 45° S (Fig. 4e), indicates that
reduced (elevated) wind speeds that occur during La Niña (El Niño) events in this region, suppress (enhance) the gas
exchange (Colberg et al., 2004) and therefore acts as a weaker (stronger) CO_2 sink. In the equatorial region, neither ΔpCO_2
or the CO_2 flux were correlated with the MEI, in sharp contrast with Lefèvre et al. (2013) who showed stronger outgassing of
CO_2 in the western equatorial Atlantic for the year following the 2009 El Niño. In that respect, it should be noted that our
analysis would not identify such lagged correlations.

The SAM has known meteorological connections to the MEI (Fogt et al., 2011), where El Niño (La Niña) events generally
coincide with negative (positive) SAM phases, resulting in northward (southward) displacement of the westerly winds in the
Southern Ocean. Our results showed positive correlations between the CO_2 flux and the SAM between 30° S and 45° S (Fig.
4f) indicating stronger (weaker) CO_2 drawdown into the oceans during negative (positive) SAM phases. Although no
significant correlations were found between ΔpCO_2 and the SAM (Fig. 3f), the changes in the gas transfer driven by the
displacement of the westerly winds could control the CO_2 flux. It should be noted that the effect of the SAM may be more
pronounced outside the domain of the present study (i.e south of 45 °S; (Keppler and Landschützer, 2019). Landschützer et
al. (2015) indicated that the SAM is unlikely to be the main driver of changes in the Southern Ocean CO_2 flux, but an
observed zonally asymmetric atmospheric pattern could induce changes in the CO_2 flux (Keppler and Landschützer, 2019;
Landschützer et al., 2015). This asymmetric atmospheric pattern, however, may not be captured within the SAM index.

4.3. Multi-year trends in ΔpCO_2 and CO_2 flux

The trends in ΔpCO_2 and CO_2 flux over 16 years (Fig. 5) showed some similarities to previous trend assessments in the
South Atlantic Ocean (Landschützer et al., 2016). Our results indicated a lower number of significant trends however, since
uncertainties in the trend analysis were accounted for. The uncertainties in both the $pCO_{2\ (sw)}$ estimates from extrapolation
techniques and the gas transfer velocity are rarely propagated through previous trend analyses. By accounting for these
uncertainties, the trend analyses provide a robust depiction of regions that can confidently be determined as changing. As
with the seasonal and inter-annual analysis, the CO_2 flux-based trend analysis showed a greater spatial area of significant
trends, when compared to ΔpCO_2 (Fig. 5).

The strongest trends in ΔpCO_2 and the CO_2 flux were observed in the Benguela upwelling system. Arnone et al. (2017)
reported positive trends in *in situ* $pCO_{2\ (sw)}$ of 6.1 ± 1.4 μatm yr^{-1}, between 2005 and 2015. Assuming an atmospheric CO_2
increase of 1.5 μatm yr^{-1} (Takahashi et al., 2002; Zeng et al., 2014), these results are consistent with the ΔpCO_2 trends
observed in this study (1.5 – 3.8 μatm yr^{-1}, Fig. 5a). Arnone et al. (2017) also suggested that the positive trend was due to a
stronger influence of upwelling (Rouault et al., 2010), which injects CO_2 and nutrients into the area that is then not
completely removed by the enhanced NPP/NCP. Varela et al. (2015) indicated an increase in the strength of the Benguela
upwelling. By contrast, Lamont et al. (2018) showed no significant change in upwelling in the Southern Benguela but

increases in the Northern Benguela which are consistent with our data that highlights an increasing efflux of CO_2 to the atmosphere (Fig. 5b). The CO_2 flux trends in this study (0.03 – 0.09 mol m^{-2} yr^{-1}, Fig. 5b) were also consistent with but slightly lower than the 0.13 ± 0.03 mol m^{-2} yr^{-1} trend in CO_2 flux observed by Arnone et al. (2017). An increase in the strength of the upwelling that injects CO_2 into the surface layer, will be driven by enhanced (upwelling-conducive) winds, that also enhance the gas transfer. This highlights the importance of studying multi-year trends using the CO_2 flux, because the enhancement of these trends by meteorological conditions would not be observed using ΔpCO_2 alone.

Offshore from the upwelling region negative ΔpCO_2 and CO_2 flux trends were observed. Rubio et al. (2009) showed that mesoscale filaments and eddies propagate away from the upwelling front, transporting nutrients offshore into the South Atlantic gyre. Ford et al. (2021b) showed negative correlations between sea level height anomalies (SLHA), and NPP/NCP anomalies (negative SLHA; positive NCP/NPP), indicating an influence of mesoscale features on ΔpCO_2 and the CO_2 flux. Xiu et al. (2018) indicated that an increase in upwelling conducive winds could increase the number of mesoscale eddies, which would transport nutrients offshore of the Californian upwelling. Although the Benguela and Californian upwelling systems are not identical, these connections could suggest an elevated nutrient export offshore, driving elevated NPP/NCP, which would increase the CO_2 sink. Kulk et al. (2020) showed significant increases in NPP of ~2 % yr^{-1}, between 1998 and 2018 in the region of strong negative trends in the CO_2 flux observed in this study, which supports the contribution of NCP to multi-year trends in the CO_2 flux.

There were also positive trends in ΔpCO_2 and CO_2 flux in the Equatorial Atlantic. In the Eastern Equatorial Atlantic, Lefèvre et al. (2016) previously suggested a negative trend in *in situ* ΔpCO_2, between 2006 and 2013, but indicated that the trend may be biased by extreme events at either end of the record. From 1995 to 2007, Parard et al. (2010) indicated a greater increase in *in situ* pCO_2 $_{(sw)}$ than pCO_2 $_{(atm)}$ (increasing ΔpCO_2), but the trend was derived from data from only two research cruises. For the Equatorial upwelling, an increase in ΔpCO_2 (as shown here and in (Landschützer et al., (2016) is counter intuitive because there is evidence that upwelled water has recently been in contact with the atmosphere (~15 years; Reverdin et al., 1993). Dissolved inorganic carbon in these upwelled waters has been shown to increase at a similar rate to the surface waters (e.g Woosley et al., 2016). Therefore, the trend in ΔpCO_2 should be ~0 with increasing pCO_2 $_{(atm)}$. This could suggest a missing component within the SA-FNN to estimate pCO_2 $_{(sw)}$, such as changes in the biological export efficiency (Kim et al., 2019), which could then suppress upwelling induced CO_2 outgassing.

The Western Tropical Atlantic, in the vicinity of the Amazon Plume, also showed positive trends in ΔpCO_2 and CO_2 flux. Previous studies have not investigated the trends in ΔpCO_2 or CO_2 flux in the Amazon Plume, however the carbon retention in a colored ocean site (CARIACO), situated to the northwest, displayed positive trends in pCO_2 $_{(sw)}$ of 2.95 ± 0.43 µatm yr^{-1} (Bates et al., 2014). Araujo et al. (2019) identified a positive trend in pCO_2 $_{(sw)}$ of 1.20 µatm yr^{-1}, but a trend in pCO_2 $_{(atm)}$ of 1.70 µatm yr^{-1} (i.e. decreasing ΔpCO_2) for the northeast Brazilian coast, Although, the air-sea CO_2 flux and ΔpCO_2 within the Amazon Plume region is spatially and temporally variable (Valerio et al., 2021; Ibánhez et al., 2016; Bruto et al., 2017).

The South Atlantic gyre exhibited negative trends in ΔpCO_2 and the CO_2 flux indicating an increasing drawdown of atmospheric CO_2 into the ocean, which were consistent with Landschützer et al. (2016) over the period from 1982 and 2011

though the trends were at the limits of the uncertainties (Fig. B2). Fay and Mckinley (2013) showed weak negative trends in $\Delta p CO_2$ using *in situ* observations over different time series lengths. Using an ensemble of complete $pCO_{2\ (sw)}$ fields, Gregor et al. (2019), with an ensemble of complete $pCO_{2\ (sw)}$ fields, indicated negative trends in $\Delta p CO_2$ however there was low confidence in these trends especially in the South Atlantic gyre. By contrast, Kitidis et al. (2017) reported a mean trend in *in situ* $\Delta p CO_2$ between 1995 and 2013, that was not significantly different from zero. These contradictory trends support the conclusion that $\Delta p CO_2$ is unlikely to be representative of the CO_2 flux over multi-year timescales. Therefore, we recommend that the CO_2 flux should be used to assess multi-year variability in the oceanic CO_2 sink, as the importance of changes in solubility and gas transfer velocity (estimated via wind speed) increases (Keppler and Landschützer, 2019).

During the United Nations decade of ocean science (2021-2030) , the Integrated Ocean Carbon Research (IOC-R) highlights that the role of biology is a key issue to understanding the global ocean CO_2 sink (Aricò et al., 2021). The biological contribution to both interannual and multi-year variations in the South Atlantic air-sea CO_2 flux shown in this study, and supported by Ford et al. (2022), indicates that the biology activity through NCP cannot be assumed to be in steady state. The biological effect of NCP on $\Delta p CO_2$ and CO_2 flux should therefore not be overlooked when assessing the interannual and multi-year variations in the global ocean carbon sink.

5. Conclusions

In this paper, we have identified the seasonal and interannual drivers of $\Delta p CO_2$ and the air-sea CO_2 flux in the South Atlantic Ocean using satellite observations. Seasonally, our results indicated that the subtropics were controlled by SST, and the subpolar regions were correlated with biological processes. Deviations from this trend occurred in the Benguela upwelling where predominately biological processes correlated with variability in the $\Delta p CO_2$ as well as upwelling. The Equatorial Atlantic showed spatially variable drivers associated with the Amazon Plume and Equatorial upwelling which induced a biological effect. These regions imply a strong biological control on $\Delta p CO_2$ through local physical processes. The CO_2 flux had similar seasonal drivers to $\Delta p CO_2$, but with significant correlations over a larger spatial area. This highlights that $\Delta p CO_2$ can be used to indicate the important drivers of the CO_2 flux on seasonal timescales, but it is still possible that $\Delta p CO_2$ will miss some of the spatial correlations and will likely overestimate the strength of these correlations.

The interannual variability of $\Delta p CO_2$ and the CO_2 flux was correlated with the MEI through a reduction (increase) of NCP and increase (decrease) in SST during El Niño (La Niña) events, again highlighting the importance of biology to the interannual variability. The CO_2 flux response extended over a larger geographical region, indicating that the CO_2 flux should be used to assess interannual trends in the oceanic CO_2 sink, as opposed to a proxy such as $\Delta p CO_2$, which may overestimate the strength of the correlations and does not include variability in the solubility and the gas transfer velocity (estimated via wind speed). The 16 year trends in $\Delta p CO_2$ and the CO_2 flux were determined with associated uncertainties which identified negative trends in the CO_2 flux in the South Atlantic gyre. Positive trends in the CO_2 flux were observed in the Benguela upwelling region, which were associated with an increase in the strength and frequency of upwelling. A

transition to negative trends offshore were consistent with elevated nutrient export from the upwelling area, and subsequent biological drawdown of CO_2. These results highlight, that changes in biological activity in the South Atlantic Ocean can control the interannual and multi-year trends in the oceanic CO_2 flux. This emphasises the importance of biology and specifically NCP in assessing the global ocean carbon sink.

Appendices

Appendix A – Driver analysis using *in situ* Δ*p*CO₂

Henson et al. (2018) performed the X-11 analysis using *in situ* $pCO_{2\ (sw)}$ observations to estimate average ΔpCO_2 for the Longhurst provinces (Longhurst, 1998). The in situ $pCO_{2\ (sw)}$ observations were obtained from SOCATv2020 (https://www.socat.info/; Bakker et al., 2016), and were reanalysed to a temperature dataset representative for a consistent and fixed depth (Reynolds et al., 2002) which is used to represent the base of the mass boundary layer. The reanalysis method used the 'fe_reanalyse_socat.py' routine within FluxEngine (Holding et al., 2019; Shutler et al., 2016), which follows the methodology of Goddijn-Murphy et al. (2015), and as used in Woolf et al. (2019) and Watson et al (2020). ΔpCO_2 was calculated using the reanalysed *in situ* $pCO_{2\ (sw)}$ observations and $pCO_{2\ (atm)}$. These ΔpCO_2 estimates were used within the driver analysis as described by Henson et al. (2018), using the drivers described in section 2.4, for the South Atlantic Longhurst provinces (Longhurst, 1998). The seasonal drivers of *in situ* ΔpCO_2 (Fig. A1) showed a similar spatial distribution as the SA-FNN ΔpCO_2 (Fig. 1). The interannual drivers (Fig. A2) showed some differences to the SA-FNN (Fig. 3). The averaging required to produce the *in situ* ΔpCO_2 timeseries may mask interannual signals, and Ford et al. (2021b) indicated that averaging over large province areas could mask correlations, especially in dynamic regions, and locally these correlations may be significant.
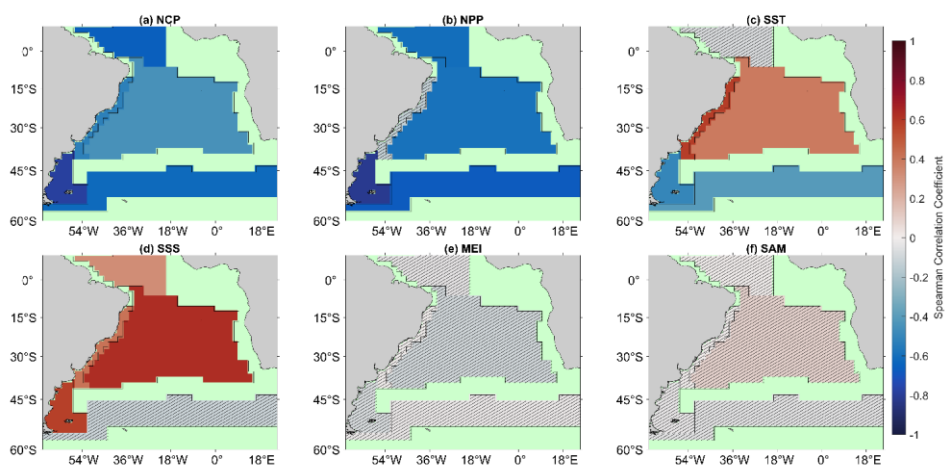
445 **Figure A1 - Spearman correlations between the *in situ* ΔpCO$_2$ seasonal component of the X-11 analysis and (a) net community production (NCP), (b) net primary production (NPP), (c) sea surface temperature (SST), (d) sea surface salinity (SSS), (e) Multivariate ENSO index (MEI) and (f) Southern Annular Mode (SAM) seasonal components on a per province basis. Hashed areas indicate no significant correlations, and green regions indicate no analysis was performed due to missing data.**

450
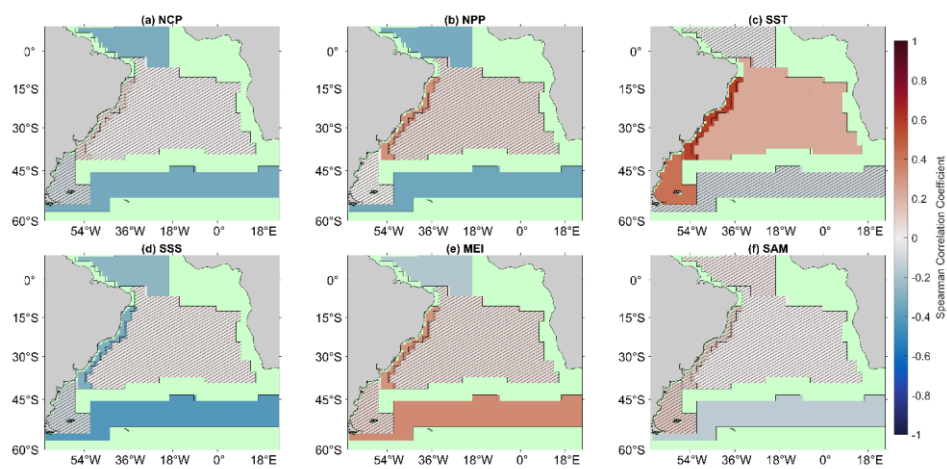
Figure A2 - Spearman correlations between the *in situ* ΔpCO₂ interannual component of the X-11 analysis and (a) net community production (NCP), (b) net primary production (NPP), (c) sea surface temperature (SST), (d) sea surface salinity (SSS) (e) Multivariate ENSO index (MEI) (f) Southern Annular Mode (SAM) interannual components on a per province basis. Hashed areas indicate no significant correlations, and green regions indicate no analysis was performed due to missing data.

Appendix B – SA-FNN $p\mathrm{CO}_{2\,(sw)}$ and trend uncertainties
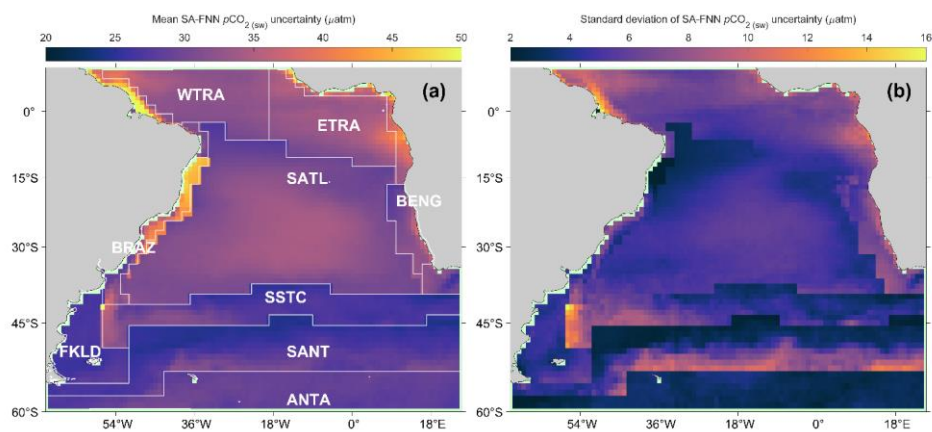
Figure B1 – (a) Mean SA-FNN $p\mathrm{CO}_{2\,(sw)}$ uncertainty between July 2002 and December 2018. Longhurst provinces (Longhurst, 1998) used within the SA-FNN training described in Ford et al. (2022; note the WTRA and ETRA are merged into one province). The province areas acronyms are listed as follows: WTRA is western tropical Atlantic; ETRA is eastern equatorial Atlantic; SATL is South Atlantic Gyre; BRAZ is Brazilian current coastal; BENG is Benguela Current coastal upwelling; FKLD is Southwest Atlantic shelves; SSTC is South Subtropical Convergence; SANT is sub-Antarctic and ANTA is Antarctic. (b) Standard deviation of SA-FNN $p\mathrm{CO}_{2\,(sw)}$ uncertainty.

460

465
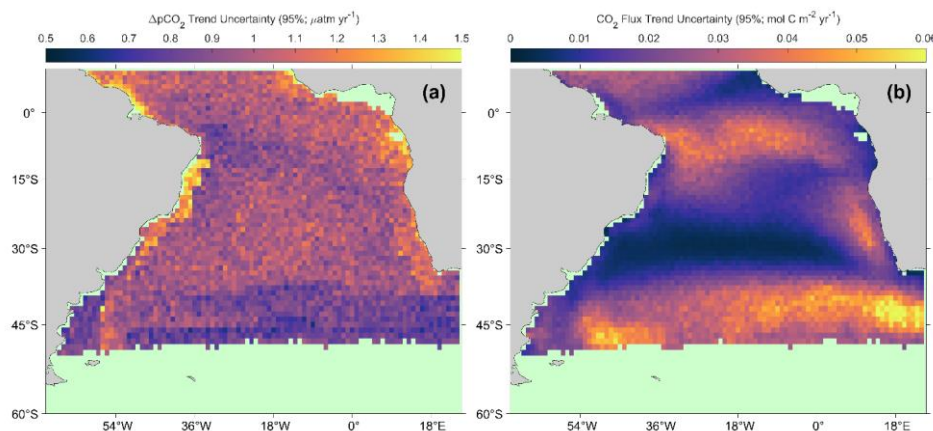
Figure B2 – (a) Uncertainty in the Δ*p*CO₂ trends presented in Fig. 5a (b) Uncertainty in the air-sea CO₂ flux trends presented in Fig. 5b

Data Availability

Moderate Resolution Imaging Spectroradiometer on Aqua (MODIS-A) estimates of chlorophyll-*a* (NASA OBPG, 2017a),
470   photosynthetically active radiation (NASA OBPG, 2017b) and sea surface temperature (NASA OBPG, 2015) are available
from the National Aeronautics Space Administration (NASA) ocean colour website (https://oceancolor.gsfc.nasa.gov/).
Modelled sea surface salinity from the Copernicus Marine Environment Modelling Service global ocean physics reanalysis
product (GLORYS12V1) are available from CMEMS (CMEMS, 2021). ERA5 monthly reanalysis wind speeds are available
from the Copernicus Climate Data Store (Hersbach et al., 2019). $pCO_{2\,(atm)}$ data are available from v5.5 of the global
475   estimates of $pCO_{2\,(sw)}$ dataset (Landschützer et al., 2017, 2016). $pCO_{2\,(sw)}$ estimates generated by the SA-FNN are available
from Pangaea (Ford et al., 2021a). SOCATv2020 *in situ* $pCO_{2\,(sw)}$ observations (Bakker et al., 2016) are available from
https://www.socat.info/index.php/version-2020/.

Author Contributions

DJF, GHT, JDS and VK conceived and directed the research. DJF developed the code and prepared the manuscript. GHT,
480   JDS and VK provided comments that shaped the final manuscript.

Competing Interests

The authors declare that they have no conflict of interest.

Acknowledgements

Daniel J. Ford was supported by a NERC GW4+ Doctoral Training Partnership studentship from the UK Natural
Environment Research Council (NERC; NE/L002434/1). Gavin H. Tilstone and Vassilis Kitidis were supported by the
AMT4CO$_2$Flux (4000125730/18/NL/FF/gp) contract from the European Space Agency and by the NERC National
Capability funding to Plymouth Marine Laboratory for the Atlantic Meridional Transect (CLASS-AMT). The Atlantic
Meridional Transect is funded by the UK Natural Environment Research Council through its National Capability Long-term
Single Centre Science Programme, Climate Linked Atlantic Sector Science (grant number NE/R015953/1). This study
contributes to the international IMBeR project and is contribution number 372 of the AMT programme. We also thank the
Natural Environment Research Council Earth Observation Data Acquisition and Analysis Service (NEODAAS) for use of
the Linux cluster to process the MODIS-A satellite imagery. We thank two anonymous reviewers for their comments, which
have improved the manuscript.

The Surface Ocean CO$_2$ Atlas (SOCAT) is an international effort, endorsed by the International Ocean Carbon Coordination
Project (IOCCP), the Surface Ocean Lower Atmosphere Study (SOLAS) and the Integrated Marine Biosphere Research
(IMBeR) program, to deliver a uniformly quality-controlled surface ocean CO$_2$ database. The many researchers and funding
agencies responsible for the collection of data and quality control are thanked for their contributions to SOCAT.

References

Aguiar, A. L., Cirano, M., Marta-Almeida, M., Lessa, G. C., and Valle-Levinson, A.: Upwelling processes along the South
Equatorial Current bifurcation region and the Salvador Canyon (13°S), Brazil, Cont. Shelf Res., 171, 77–96,
https://doi.org/10.1016/j.csr.2018.10.001, 2018.

Araujo, M., Noriega, C., Medeiros, C., Lefèvre, N., Ibánhez, J. S. P., Flores Montes, M., Silva, A. C. da, and Santos, M. de
L.: On the variability in the CO$_2$ system and water productivity in the western tropical Atlantic off North and Northeast
Brazil, J. Mar. Syst., 189, 62–77, https://doi.org/10.1016/j.jmarsys.2018.09.008, 2019.

Aricò, S., Arrieta, J. M., Bakker, D. C. E., Boyd, P. W., Cotrim da Cunha, L., Chai, F., Dai, M., Gruber, N., Isensee, K.,
Ishii, M., Jiao, N., Lauvset, S. K., McKinley, G. A., Monteiro, P., Robinson, C., Sabine, C., Sanders, R., Schoo, K. L.,
Schuster, U., Shutler, J. D., Thomas, H., Wanninkhof, R., Watson, A. J., Bopp, L., Boss, E., Bracco, A., Cai, W., Fay, A.,
Feely, R. A., Gregor, L., Hauck, J., Heinze, C., Henson, S., Hwang, J., Post, J., Suntharalingam, P., Telszewski, M.,
Tilbrook, B., Valsala, V., and Rojas, A.: Integrated Ocean Carbon Research: A Summary of Ocean Carbon Research, and

Vision of Coordinated Ocean Carbon Research and Observations for the Next Decade., edited by: Wanninkhof, R., Sabine, C., and Aricò, S., UNESCO, Paris, 46 pp., https://doi.org/10.25607/h0gj-pq41, 2021.

Arnone, V., González-Dávila, M., and Magdalena Santana-Casiano, J.: CO_2 fluxes in the South African coastal region, Mar. Chem., 195, 41–49, https://doi.org/10.1016/j.marchem.2017.07.008, 2017.

515 Bakker, D. C. E., Pfeil, B., Landa, C. S., Metzl, N., O'Brien, K. M., Olsen, A., Smith, K., Cosca, C., Harasawa, S., Jones, S. D., Nakaoka, S. I., Nojiri, Y., Schuster, U., Steinhoff, T., Sweeney, C., Takahashi, T., Tilbrook, B., Wada, C., Wanninkhof, R., Alin, S. R., Balestrini, C. F., Barbero, L., Bates, N. R., Bianchi, A. A., Bonou, F., Boutin, J., Bozec, Y., Burger, E. F., Cai, W. J., Castle, R. D., Chen, L., Chierici, M., Currie, K., Evans, W., Featherstone, C., Feely, R. A., Fransson, A., Goyet, C., Greenwood, N., Gregor, L., Hankin, S., Hardman-Mountford, N. J., Harlay, J., Hauck, J., Hoppema, M., Humphreys, M.

520 P., Hunt, C. W., Huss, B., Ibánhez, J. S. P., Johannessen, T., Keeling, R., Kitidis, V., Körtzinger, A., Kozyr, A., Krasakopoulou, E., Kuwata, A., Landschützer, P., Lauvset, S. K., Lefèvre, N., Lo Monaco, C., Manke, A., Mathis, J. T., Merlivat, L., Millero, F. J., Monteiro, P. M. S., Munro, D. R., Murata, A., Newberger, T., Omar, A. M., Ono, T., Paterson, K., Pearce, D., Pierrot, D., Robbins, L. L., Saito, S., Salisbury, J., Schlitzer, R., Schneider, B., Schweitzer, R., Sieger, R., Skjelvan, I., Sullivan, K. F., Sutherland, S. C., Sutton, A. J., Tadokoro, K., Telszewski, M., Tuma, M., Van Heuven, S. M. A.

525 C., Vandemark, D., Ward, B., Watson, A. J., and Xu, S.: A multi-decade record of high-quality fCO_2 data in version 3 of the Surface Ocean CO_2 Atlas (SOCAT), Earth Syst. Sci. Data, 8, 383–413, https://doi.org/10.5194/essd-8-383-2016, 2016.

Bates, N. R., Astor, Y. M., Church, M. J., Currie, K., Dore, J. E., González-Dávila, M., Lorenzoni, L., Muller-Karger, F., Olafsson, J., and Santana-Casiano, J. M.: A time-series view of changing surface ocean chemistry due to ocean uptake of anthropogenic CO_2 and ocean acidification, 27, 126–141, https://doi.org/10.5670/oceanog.2014.16, 2014.

530 Bonou, F. K., Noriega, C., Lefèvre, N., and Araujo, M.: Distribution of CO_2 parameters in the Western Tropical Atlantic Ocean, Dyn. Atmos. Ocean., 73, 47–60, https://doi.org/10.1016/j.dynatmoce.2015.12.001, 2016.

Bruto, L., Araujo, M., Noriega, C., Veleda, D., and Lefèvre, N.: Variability of CO_2 fugacity at the western edge of the tropical Atlantic Ocean from the 8°N to 38°W PIRATA buoy, Dyn. Atmos. Ocean., 78, 1–13, https://doi.org/10.1016/j.dynatmoce.2017.01.003, 2017.

535 CMEMS: Copernicus Marine Modelling Service global ocean physics reanalysis product (GLORYS12V1), Copernicus Mar. Model. Serv. [data set], https://doi.org/10.48670/moi-00021, 2021.

Colberg, F., Reason, C. J. C., and Rodgers, K.: South Atlantic response to El Niño-Southern Oscillation induced climate variability in an ocean general circulation model, J. Geophys. Res. C Ocean., 109, 1–14, https://doi.org/10.1029/2004JC002301, 2004.

540 Cooley, S. R., Coles, V. J., Subramaniam, A., and Yager, P. L.: Seasonal variations in the Amazon plume-related atmospheric carbon sink, Global Biogeochem. Cycles, 21, 1–15, https://doi.org/10.1029/2006GB002831, 2007.

Dickson, A. G., Sabine, C. L., and Christian, J. R.: Guide to Best Practices for Ocean CO_2 measurements., 191 pp. pp., 2007.

Dong, Y., Yang, M., Bakker, D. C. E., Kitidis, V., and Bell, T. G.: Uncertainties in eddy covariance air–sea CO_2 flux measurements and implications for gas transfer velocity parameterisations, Atmos. Chem. Phys., 21, 8089–8110,

545 https://doi.org/10.5194/acp-21-8089-2021, 2021.

Donlon, C. J., Nightingale, T. J., Sheasby, T., Turner, J., Robinson, I. S., and Emergy, W. J.: Implications of the oceanic thermal skin temperature deviation at high wind speed, Geophys. Res. Lett., 26, 2505–2508, https://doi.org/10.1029/1999GL900547, 1999.

Fay, A. R. and McKinley, G. A.: Global trends in surface ocean pCO_2 from in situ data, Global Biogeochem. Cycles, 27, 550 541–557, https://doi.org/10.1002/gbc.20051, 2013.

Fogt, R. L., Bromwich, D. H., and Hines, K. M.: Understanding the SAM influence on the South Pacific ENSO teleconnection, Clim. Dyn., 36, 1555–1576, https://doi.org/10.1007/s00382-010-0905-0, 2011.

Ford, D., Tilstone, G. H., Shutler, J. D., Kitidis, V., Lobanova, P., Schwarz, J., Poulton, A. J., Serret, P., Lamont, T., Chuqui, M., Barlow, R., Lozano, J., Kampel, M., and Brandini, F.: Wind speed and mesoscale features drive net autotrophy in the 555 South Atlantic Ocean, Remote Sens. Environ., 260, 112435, https://doi.org/10.1016/j.rse.2021.112435, 2021ba.

Ford, D. J., Tilstone, G. H., Shutler, J. D., and Kitidis, V.: Interpolated surface ocean carbon dioxide partial pressure for the South Atlantic Ocean (2002-2018) using different biological parameters, PANGAEA [data set], https://doi.org/10.1594/PANGAEA.935936, 2021ab.

Ford, D. J., Tilstone, G. H., Shutler, J. D., and Kitidis, V.: Derivation of seawater pCO_2 from net community production 560 identifies the South Atlantic Ocean as a CO_2 source, 19, 93–115, https://doi.org/10.5194/bg-19-93-2022, 2022.

Friedlingstein, P., O'Sullivan, M., Jones, M. W., Andrew, R. M., Hauck, J., Olsen, A., Peters, G. P., Peters, W., Pongratz, J., Sitch, S., Le Quéré, C., Canadell, J. G., Ciais, P., Jackson, R. B., Alin, S., Aragão, L. E. O. C., Arneth, A., Arora, V., Bates, N. R., Becker, M., Benoit-Cattin, A., Bittig, H. C., Bopp, L., Bultan, S., Chandra, N., Chevallier, F., Chini, L. P., Evans, W., Florentie, L., Forster, P. M., Gasser, T., Gehlen, M., Gilfillan, D., Gkritzalis, T., Gregor, L., Gruber, N., Harris, I., Hartung, 565 K., Haverd, V., Houghton, R. A., Ilyina, T., Jain, A. K., Joetzjer, E., Kadono, K., Kato, E., Kitidis, V., Korsbakken, J. I., Landschützer, P., Lefèvre, N., Lenton, A., Lienert, S., Liu, Z., Lombardozzi, D., Marland, G., Metzl, N., Munro, D. R., Nabel, J. E. M. S., Nakaoka, S.-I., Niwa, Y., O'Brien, K., Ono, T., Palmer, P. I., Pierrot, D., Poulter, B., Resplandy, L., Robertson, E., Rödenbeck, C., Schwinger, J., Séférian, R., Skjelvan, I., Smith, A. J. P., Sutton, A. J., Tanhua, T., Tans, P. P., Tian, H., Tilbrook, B., van der Werf, G., Vuichard, N., Walker, A. P., Wanninkhof, R., Watson, A. J., Willis, D., Wiltshire, 570 A. J., Yuan, W., Yue, X., and Zaehle, S.: Global Carbon Budget 2020, Earth Syst. Sci. Data, 12, 3269–3340, https://doi.org/10.5194/essd-12-3269-2020, 2020.

Goddijn-Murphy, L. M., Woolf, D. K., Land, P. E., Shutler, J. D., and Donlon, C.: The OceanFlux Greenhouse Gases methodology for deriving a sea surface climatology of CO_2 fugacity in support of air-sea gas flux studies, Ocean Sci., 11, 519–541, https://doi.org/10.5194/os-11-519-2015, 2015.

575 González-Dávila, M., Santana-Casiano, J. M., and Ucha, I. R.: Seasonal variability of fCO_2 in the Angola-Benguela region, Prog. Oceanogr., 83, 124–133, https://doi.org/10.1016/j.pocean.2009.07.033, 2009.

Gregor, L., Lebehot, A. D., Kok, S., and Scheel Monteiro, P. M.: A comparative assessment of the uncertainties of global surface ocean CO_2 estimates using a machine-learning ensemble (CSIR-ML6 version 2019a)-Have we hit the wall?, Geosci.

Model Dev., 12, 5113–5136, https://doi.org/10.5194/gmd-12-5113-2019, 2019.

580   Henson, S. A., Humphreys, M. P., Land, P. E., Shutler, J. D., Goddijn-Murphy, L., and Warren, M.: Controls on Open-Ocean North Atlantic ΔpCO_2 at Seasonal and Interannual Time Scales Are Different, Geophys. Res. Lett., 45, 9067–9076, https://doi.org/10.1029/2018GL078797, 2018.

Hersbach, H., Bell, B., Berrisford, P., Biavati, G., Horányi, A., Muñoz Sabater, J., Nicolas, J., Peubey, C., Radu, R., Rozum, I., Schepers, D., Simmons, A., Soci, C., Dee, D., and Thépaut, J.-N.: ERA5 monthly averaged data on single levels from

585   1979 to present, Copernicus Clim. Chang. Serv. Clim. Data Store [dataset], https://doi.org/10.24381/cds.f17050d7, 2019.

Ho, D. T., Law, C. S., Smith, M. J., Schlosser, P., Harvey, M., and Hill, P.: Measurements of air-sea gas exchange at high wind speeds in the Southern Ocean: Implications for global parameterizations, Geophys. Res. Lett., 33, L16611, https://doi.org/10.1029/2006GL026817, 2006.

Holding, T., Ashton, I. G., Shutler, J. D., Land, P. E., Nightingale, P. D., Rees, A. P., Brown, I., Piolle, J.-F., Kock, A.,

590   Bange, H. W., Woolf, D. K., Goddijn-Murphy, L., Pereira, R., Paul, F., Girard-Ardhuin, F., Chapron, B., Rehder, G., Ardhuin, F., and Donlon, C. J.: The FluxEngine air–sea gas flux toolbox: simplified interface and extensions for in situ analyses and multiple sparingly soluble gases, Ocean Sci., 15, 1707–1728, https://doi.org/10.5194/os-15-1707-2019, 2019.

Hopkins, J., Lucas, M., Dufau, C., Sutton, M., Stum, J., Lauret, O., and Channelliere, C.: Detection and variability of the Congo River plume from satellite derived sea surface temperature, salinity, ocean colour and sea level, Remote Sens.

595   Environ., 139, 365–385, https://doi.org/10.1016/j.rse.2013.08.015, 2013.

Hu, C., Lee, Z., and Franz, B.: Chlorophyll a algorithms for oligotrophic oceans: A novel approach based on three-band reflectance difference, J. Geophys. Res. Ocean., 117, 1–25, https://doi.org/10.1029/2011JC007395, 2012.

Ibánhez, J. S. P., Araujo, M., and Lefèvre, N.: The overlooked tropical oceanic CO_2 sink, Geophys. Res. Lett., 43, 3804–3812, https://doi.org/10.1002/2016GL068020, 2016.

600   IPCC: Climate Change 2021: The Physical Science Basis. Contribution of Working Group I to the Sixth Assessment Report of the Intergovernmental Panel on Climate Change, edited by: Masson-Delmotte, V., Zhai, P., Pirani, A., Connors, S. L., Péan, C., Berger, S., Caud, N., Chen, Y., Goldfarb, L., Gomis, M. I., Huang, M., Leitzell, K., Lonnoy, E., Matthews, J. B. R., Maycock, T. K., Waterfield, T., Yelekçi, O., Yu, R., and Zhou, B., Cambridge University Press, 2021.

Jean-Michel, L., Eric, G., Romain, B.-B., Gilles, G., Angélique, M., Marie, D., Clément, B., Mathieu, H., Olivier, L. G.,

605   Charly, R., Tony, C., Charles-Emmanuel, T., Florent, G., Giovanni, R., Mounir, B., Yann, D., and Pierre-Yves, L. T.: The Copernicus Global 1/12° Oceanic and Sea Ice GLORYS12 Reanalysis, Front. Earth Sci., 9, 1–27, https://doi.org/10.3389/feart.2021.698876, 2021.

Kendall, M. G.: Rank Correlation Methods, 4th ed., Charles Griffin, London, UK, 1975.

Keppler, L. and Landschützer, P.: Regional Wind Variability Modulates the Southern Ocean Carbon Sink, Sci. Rep., 9, 1–

610   10, https://doi.org/10.1038/s41598-019-43826-y, 2019.

Kim, H. J., Kim, T., Hyeong, K., Yeh, S., Park, J., Yoo, C. M., and Hwang, J.: Suppressed CO_2 Outgassing by an Enhanced Biological Pump in the Eastern Tropical Pacific, J. Geophys. Res. Ocean., 124, 7962–7973,

https://doi.org/10.1029/2019JC015287, 2019.

Kitidis, V., Brown, I., Hardman-mountford, N., and Lefèvre, N.: Surface ocean carbon dioxide during the Atlantic Meridional Transect (1995 – 2013); evidence of ocean acidification, Prog. Oceanogr., 158, 65–75, https://doi.org/10.1016/j.pocean.2016.08.005, 2017.

Körtzinger, A.: A significant CO_2 sink in the tropical Atlantic Ocean associated with the Amazon River plume, Geophys. Res. Lett., 30, 2–5, https://doi.org/10.1029/2003GL018841, 2003.

Kulk, G., Platt, T., Dingle, J., Jackson, T., Jönsson, B. F., Bouman, H. A., Babin, M., Brewin, R. J. W., Doblin, M., Estrada, M., Figueiras, F. G., Furuya, K., González-Benítez, N., Gudfinnsson, H. G., Gudmundsson, K., Huang, B., Isada, T., Kovač, Ž., Lutz, V. A., Marañón, E., Raman, M., Richardson, K., Rozema, P. D., van de Poll, W. H., Segura, V., Tilstone, G. H., Uitz, J., van Dongen-Vogels, V., Yoshikawa, T., and Sathyendranath, S.: Primary production, an index of climate change in the ocean: Satellite-based estimates over two decades, Remote Sens., 12, https://doi.org/10.3390/rs12050826, 2020.

Lamont, T., Barlow, R. G., and Kyewalyanga, M. S.: Physical drivers of phytoplankton production in the southern Benguela upwelling system, Deep. Res. Part I Oceanogr. Res. Pap., 90, 1–16, https://doi.org/10.1016/j.dsr.2014.03.003, 2014.

Lamont, T., García-Reyes, M., Bograd, S. J., van der Lingen, C. D., and Sydeman, W. J.: Upwelling indices for comparative ecosystem studies: Variability in the Benguela Upwelling System, J. Mar. Syst., 188, 3–16, https://doi.org/10.1016/j.jmarsys.2017.05.007, 2018.

Landschützer, P., Gruber, N., Bakker, D. C. E., Schuster, U., Nakaoka, S., Payne, M. R., Sasse, T. P., and Zeng, J.: A neural network-based estimate of the seasonal to inter-annual variability of the Atlantic Ocean carbon sink, 10, 7793–7815, https://doi.org/10.5194/bg-10-7793-2013, 2013.

Landschützer, P., Gruber, N., Bakker, D. C. E., and Schuster, U.: Recent variability of the global ocean carbon sink, Global Biogeochem. Cycles, 28, 927–949, https://doi.org/10.1002/2014GB004853, 2014.

Landschützer, P., Gruber, N., Haumann, F. A., Rödenbeck, C., Bakker, D. C. E., van Heuven, S., Hoppema, M., Metzl, N., Sweeney, C., Takahashi, T., Tilbrook, B., and Wanninkhof, R.: The reinvigoration of the Southern Ocean carbon sink, Science (80-.)., 349, 1221–1224, https://doi.org/10.1126/science.aab2620, 2015.

Landschützer, P., Gruber, N., and Bakker, D. C. E.: Decadal variations and trends of the global ocean carbon sink, Global Biogeochem. Cycles, 30, 1396–1417, https://doi.org/10.1002/2015GB005359, 2016.

Landschützer, P., Gruber, N., and Bakker, D. C. E.: An observation-based global monthly gridded sea surface pCO2 product from 1982 onward and its monthly climatology (NCEI Accession 0160558), NOAA Natl. Centers Environ. Information. Dataset, https://doi.org/10.7289/v5z899n6, 2017.

Lefévre, N., Diverrés, D., and Gallois, F.: Origin of CO_2 undersaturation in the western tropical Atlantic, Tellus, Ser. B Chem. Phys. Meteorol., 62, 595–607, https://doi.org/10.1111/j.1600-0889.2010.00475.x, 2010.

Lefèvre, N., Guillot, A., Beaumont, L., and Danguy, T.: Variability of fCO2 in the Eastern Tropical Atlantic from a moored buoy, J. Geophys. Res. Ocean., 113, https://doi.org/10.1029/2007JC004146, 2008.

Lefèvre, N., Caniaux, G., Janicot, S., and Gueye, A. K.: Increased CO_2 outgassing in February-May 2010 in the tropical

Atlantic following the 2009 Pacific El Niño, J. Geophys. Res. Ocean., 118, 1645–1657, https://doi.org/10.1002/jgrc.20107, 2013.

Lefèvre, N., Veleda, D., Araujo, M., and Caniaux, G.: Variability and trends of carbon parameters at a time series in the eastern tropical Atlantic, Tellus, Ser. B Chem. Phys. Meteorol., 68, https://doi.org/10.3402/tellusb.v68.30305, 2016.

Lefèvre, N., Tyaquiçã, P., Veleda, D., Perruche, C., and van Gennip, S. J.: Amazon River propagation evidenced by a CO_2 decrease at 8°N, 38°W in September 2013, J. Mar. Syst., 211, 103419, https://doi.org/10.1016/j.jmarsys.2020.103419, 2020.

Lefèvre, N., Mejia, C., Khvorostyanov, D., Beaumont, L., and Koffi, U.: Ocean Circulation Drives the Variability of the Carbon System in the Eastern Tropical Atlantic, 2, 126–148, https://doi.org/10.3390/oceans2010008, 2021.

Liutti, C. C., Kerr, R., Monteiro, T., Orselli, I. B. M., Ito, R. G., and Garcia, C. A. E.: Sea surface CO_2 fugacity in the southwestern South Atlantic Ocean: An evaluation based on satellite-derived images, Mar. Chem., 236, 104020, https://doi.org/10.1016/j.marchem.2021.104020, 2021.

Longhurst, A.: Ecological geography of the sea, Academic Press, San Diego, 1998.

Mann, H. B.: Nonparametric Tests Against Trend, 13, 245, https://doi.org/10.2307/1907187, 1945.

Mason, E., Pascual, A., Gaube, P., Ruiz, S., Pelegrí, J. L., and Delepoulle, A.: Subregional characterization of mesoscale eddies across the Brazil-Malvinas Confluence, J. Geophys. Res. Ocean., 122, 3329–3357, https://doi.org/10.1002/2016JC012611, 2017.

Morel, A.: Light and marine photosynthesis: a spectral model with geochemical and climatological implications, Prog. Oceanogr., 26, 263–306, https://doi.org/10.1016/0079-6611(91)90004-6, 1991.

NASA OBPG: MODIS Aqua Level 3 SST Thermal IR Daily 4km Daytime v2014.0, NASA Phys. Oceanogr. DAAC [data set], https://doi.org/10.5067/MODSA-1D4D4, 2015.

NASA OBPG: MODIS-Aqua Level 3 Mapped Chlorophyll Data Version R2018.0, NASA Ocean Biol. DAAC [data set], https://doi.org/10.5067/AQUA/MODIS/L3M/CHL/2018, 2017a.

NASA OBPG: MODIS-Aqua Level 3 Mapped Photosynthetically Available Radiation Data Version R2018.0, NASA Ocean Biol. DAAC [data set], https://doi.org/10.5067/AQUA/MODIS/L3M/PAR/2018, 2017b.

Nightingale, P. D., Malin, G., Law, C. S., Watson, A. J., Liss, P. S., Liddicoat, M. I., Boutin, J., and Upstill-Goddard, R. C.: In situ evaluation of air-sea gas exchange parameterizations using novel conservative and volatile tracers, Global Biogeochem. Cycles, 14, 373–387, https://doi.org/10.1029/1999GB900091, 2000.

O'Reilly, J. E. and Werdell, P. J.: Chlorophyll algorithms for ocean color sensors - OC4, OC5 & OC6, Remote Sens. Environ., 229, 32–47, https://doi.org/10.1016/j.rse.2019.04.021, 2019.

O'Reilly, J. E., Maritorena, S., Mitchell, B. G., Siegel, D. A., Carder, K. L., Garver, S. A., Kahru, M., and Mcclain, C.: Ocean color chlorophyll algorithms for SeaWiFS encompassing chlorophyll concentrations between, J. Geophys. Res., 103, 24937–24953, 1998.

Parard, G., Lefévre, N., and Boutin, J.: Sea water fugacity of CO_2 at the PIRATA mooring at 6°S, 10°W, Tellus, Ser. B Chem. Phys. Meteorol., 62, 636–648, https://doi.org/10.1111/j.1600-0889.2010.00503.x, 2010.

Pezzulli, S., Stephenson, D. B., and Hannachi, A.: The variability of seasonality, J. Clim., 18, 71–88, https://doi.org/10.1175/JCLI-3256.1, 2005.

Radenac, M. H., Jouanno, J., Carine Tchamabi, C., Awo, M., Bourlès, B., Arnault, S., and Aumont, O.: Physical drivers of the nitrate seasonal variability in the Atlantic cold tongue, 17, 529–545, https://doi.org/10.5194/bg-17-529-2020, 2020.

685 Reboita, M. S., Ambrizzi, T., Silva, B. A., Pinheiro, R. F., and da Rocha, R. P.: The south atlantic subtropical anticyclone: Present and future climate, Front. Earth Sci., 7, 1–15, https://doi.org/10.3389/feart.2019.00008, 2019.

Reverdin, G., Weiss, R. F., and Jenkins, W. J.: Ventilation of the Atlantic Ocean equatorial thermocline, J. Geophys. Res., 98, 16289, https://doi.org/10.1029/93JC00976, 1993.

Reynolds, R. W., Rayner, N. A., Smith, T. M., Stokes, D. C., and Wang, W.: An improved in situ and satellite SST analysis 690 for climate, J. Clim., 15, 1609–1625, https://doi.org/10.1175/1520-0442(2002)015<1609:AIISAS>2.0.CO;2, 2002.

Rodrigues, R. R., Campos, E. J. D., and Haarsma, R.: The impact of ENSO on the south Atlantic subtropical dipole mode, J. Clim., 28, 2691–2705, https://doi.org/10.1175/JCLI-D-14-00483.1, 2015.

Rouault, M., Pohl, B., and Penven, P.: Coastal oceanic climate change and variability from 1982 to 2009 around South Africa, African J. Mar. Sci., 32, 237–246, https://doi.org/10.2989/1814232x.2010.501563, 2010.

695 Rubio, A., Blanke, B., Speich, S., Grima, N., and Roy, C.: Mesoscale eddy activity in the southern Benguela upwelling system from satellite altimetry and model data, Prog. Oceanogr., 83, 288–295, https://doi.org/10.1016/j.pocean.2009.07.029, 2009.

Sabine, C. L., Hankin, S., Koyuk, H., Bakker, D. C. E., Pfeil, B., Olsen, A., Metzl, N., Kozyr, A., Fassbender, A., Manke, A., Malczyk, J., Akl, J., Alin, S. R., Bellerby, R. G. J., Borges, A., Boutin, J., Brown, P. J., Cai, W. J., Chavez, F. P., Chen, 700 A., Cosca, C., Feely, R. A., González-Dávila, M., Goyet, C., Hardman-Mountford, N., Heinze, C., Hoppema, M., Hunt, C. W., Hydes, D., Ishii, M., Johannessen, T., Key, R. M., Körtzinger, A., Landschützer, P., Lauvset, S. K., Lefèvre, N., Lenton, A., Lourantou, A., Merlivat, L., Midorikawa, T., Mintrop, L., Miyazaki, C., Murata, A., Nakadate, A., Nakano, Y., Nakaoka, S., Nojiri, Y., Omar, A. M., Padin, X. A., Park, G. H., Paterson, K., Perez, F. F., Pierrot, D., Poisson, A., Ríos, A. F., Salisbury, J., Santana-Casiano, J. M., S. Sarma, V. V. S., Schlitzer, R., Schneider, B., Schuster, U., Sieger, R., Skjelvan, I., 705 Steinhoff, T., Suzuki, T., Takahashi, T., Tedesco, K., Telszewski, M., Thomas, H., Tilbrook, B., Vandemark, D., Veness, T., Watson, A. J., Weiss, R., Wong, C. S., and Yoshikawa-Inoue, H.: Surface Ocean CO_2 Atlas (SOCAT) gridded data products, Earth Syst. Sci. Data, 5, 145–153, https://doi.org/10.5194/essd-5-145-2013, 2013.

Santana-Casiano, J. M., González-Dávila, M., and Ucha, I. R.: Carbon dioxide fluxes in the Benguela upwelling system during winter and spring: A comparison between 2005 and 2006, Deep Sea Res. Part II Top. Stud. Oceanogr., 56, 533–541, 710 https://doi.org/10.1016/j.dsr2.2008.12.010, 2009.

Sen, P. K.: Estimates of the Regression Coefficient Based on Kendall's Tau, J. Am. Stat. Assoc., 63, 1379–1389, https://doi.org/10.1080/01621459.1968.10480934, 1968.

Shiskin, J., Young, A. J., and Musgrave, J. C.: The X-11 variant of the Census Method II Seasonal Adjustment Program, US Dept of Commerce, 68 pp., 1967.

715 Shutler, J. D., Land, P. E., Piolle, J. F., Woolf, D. K., Goddijn-Murphy, L., Paul, F., Girard-Ardhuin, F., Chapron, B., and Donlon, C. J.: FluxEngine: A flexible processing system for calculating atmosphere-ocean carbon dioxide gas fluxes and climatologies, J. Atmos. Ocean. Technol., 33, 741–756, https://doi.org/10.1175/JTECH-D-14-00204.1, 2016.

Smyth, T. J., Tilstone, G. H., and Groom, S. B.: Integration of radiative transfer into satellite models of ocean primary production, J. Geophys. Res. C Ocean., 110, 1–11, https://doi.org/10.1029/2004JC002784, 2005.

720 Takahashi, T., Sutherland, S. C., Sweeney, C., Poisson, A., Metzl, N., Tilbrook, B., Bates, N., Wanninkhof, R., Feely, R. A., Sabine, C., Olafsson, J., and Nojiri, Y.: Global sea–air CO_2 flux based on climatological surface ocean pCO_2, and seasonal biological and temperature effects, Deep Sea Res. Part II Top. Stud. Oceanogr., 49, 1601–1622, https://doi.org/10.1016/S0967-0645(02)00003-6, 2002.

Takahashi, T., Sutherland, S. C., Wanninkhof, R., Sweeney, C., Feely, R. A., Chipman, D. W., Hales, B., Friederich, G.,
725 Chavez, F., Sabine, C., Watson, A., Bakker, D. C. E., Schuster, U., Metzl, N., Yoshikawa-Inoue, H., Ishii, M., Midorikawa, T., Nojiri, Y., Körtzinger, A., Steinhoff, T., Hoppema, M., Olafsson, J., Arnarson, T. S., Tilbrook, B., Johannessen, T., Olsen, A., Bellerby, R., Wong, C. S., Delille, B., Bates, N. R., and de Baar, H. J. W.: Climatological mean and decadal change in surface ocean pCO_2, and net sea-air CO_2 flux over the global oceans, Deep. Res. Part II Top. Stud. Oceanogr., 56, 554–577, https://doi.org/10.1016/j.dsr2.2008.12.009, 2009.

730 Tilstone, G. H., Smyth, T. J., Gowen, R. J., Martinez-Vicente, V., and Groom, S. B.: Inherent optical properties of the Irish Sea and their effect on satellite primary production algorithms, J. Plankton Res., 27, 1127–1148, https://doi.org/10.1093/plankt/fbi075, 2005.

Tilstone, G. H., Smyth, T., Poulton, A., and Hutson, R.: Measured and remotely sensed estimates of primary production in the Atlantic Ocean from 1998 to 2005, Deep. Res. Part II Top. Stud. Oceanogr., 56, 918–930,
735 https://doi.org/10.1016/j.dsr2.2008.10.034, 2009.

Tilstone, G. H., Xie, Y. yuan, Robinson, C., Serret, P., Raitsos, D. E., Powell, T., Aranguren-Gassis, M., Garcia-Martin, E. E., and Kitidis, V.: Satellite estimates of net community production indicate predominance of net autotrophy in the Atlantic Ocean, Remote Sens. Environ., 164, 254–269, https://doi.org/10.1016/j.rse.2015.03.017, 2015.

Valerio, A. M., Kampel, M., Ward, N. D., Sawakuchi, H. O., Cunha, A. C., and Richey, J. E.: CO_2 partial pressure and
740 fluxes in the Amazon River plume using in situ and remote sensing data, Cont. Shelf Res., 215, 104348, https://doi.org/10.1016/j.csr.2021.104348, 2021.

Varela, R., Álvarez, I., Santos, F., DeCastro, M., and Gómez-Gesteira, M.: Has upwelling strengthened along worldwide coasts over 1982-2010?, Sci. Rep., 5, 1–15, https://doi.org/10.1038/srep10016, 2015.

Wanninkhof, R.: Relationship between wind speed and gas exchange over the ocean revisited, Limnol. Oceanogr. Methods,
745 12, 351–362, https://doi.org/10.4319/lom.2014.12.351, 2014.

Watson, A. J., Schuster, U., Shutler, J. D., Holding, T., Ashton, I. G. C., Landschützer, P., Woolf, D. K., and Goddijn-Murphy, L.: Revised estimates of ocean-atmosphere CO_2 flux are consistent with ocean carbon inventory, Nat. Commun., 11, 1–6, https://doi.org/10.1038/s41467-020-18203-3, 2020.

Weiss, R. F.: Carbon dioxide in water and seawater: the solubility of a non-ideal gas, Mar. Chem., 2, 203–215,
750   https://doi.org/10.1016/0304-4203(74)90015-2, 1974.

Wilks, D. S.: On "field significance" and the false discovery rate, J. Appl. Meteorol. Climatol., 45, 1181–1189,
https://doi.org/10.1175/JAM2404.1, 2006.

Woolf, D. K., Land, P. E., Shutler, J. D., Goddijn-Murphy, L. M., and Donlon, C. J.: On the calculation of air-sea fluxes of
CO_2 in the presence of temperature and salinity gradients, J. Geophys. Res. Ocean., 121, 1229–1248,
755   https://doi.org/10.1002/2015JC011427, 2016.

Woolf, D. K., Shutler, J. D., Goddijn-Murphy, L., Watson, A. J., Chapron, B., Nightingale, P. D., Donlon, C. J., Piskozub, J.,
Yelland, M. J., Ashton, I., Holding, T., Schuster, U., Girard-Ardhuin, F., Grouazel, A., Piolle, J. F., Warren, M., Wrobel-
Niedzwiecka, I., Land, P. E., Torres, R., Prytherch, J., Moat, B., Hanafin, J., Ardhuin, F., and Paul, F.: Key Uncertainties in
the Recent Air-Sea Flux of CO_2, Global Biogeochem. Cycles, 33, 1548–1563, https://doi.org/10.1029/2018GB006041, 2019.
760   Woosley, R. J., Millero, F. J., and Wanninkhof, R.: Rapid anthropogenic changes in CO_2 and pH in the Atlantic Ocean:
2003-2014, Global Biogeochem. Cycles, 30, 70–90, https://doi.org/10.1002/2015GB005248, 2016.

Xiong, X., Masuda, Y., Hashioka, T., Ono, T., and Yamanaka, Y.: Effect of seasonal change in gas transfer coefficient on
air–sea CO_2 flux in the western North Pacific, J. Oceanogr., 71, 685–701, https://doi.org/10.1007/s10872-015-0313-5, 2015.

Xiu, P., Chai, F., Curchitser, E. N., and Castruccio, F. S.: Future changes in coastal upwelling ecosystems with global
765   warming: The case of the California Current System, Sci. Rep., 8, 1–9, https://doi.org/10.1038/s41598-018-21247-7, 2018.

Zeng, J., Nojiri, Y., Landschützer, P., Telszewski, M., and Nakaoka, S.: A global surface ocean fCO2 climatology based on a
feed-forward neural network, J. Atmos. Ocean. Technol., 31, 1838–1849, https://doi.org/10.1175/JTECH-D-13-00137.1,
2014.